Supporting Information for

Rational Synthesis and Characterization of Dimolybdenum(II)

Compounds Bearing Fc-containing Ligands towards Modulation

of Electronic Coupling

Xu-Min Cai,[†] Korbinian Riener,[†] Eberhardt Herdtweck,

Alexander Pöthig and Fritz E. Kühn*

Content:

01. Molecular Structures, Crystal Data and Refinement
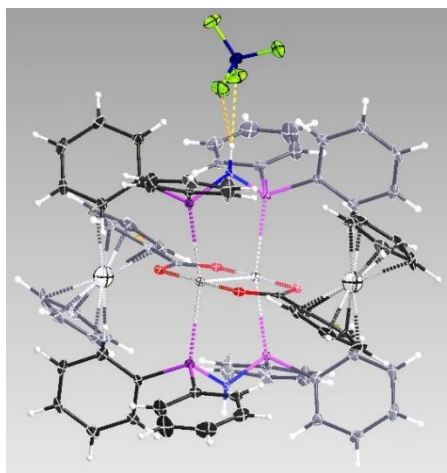

Figure S1. Molecular structure of compound **2a**.

The crystal structure could be refined up to a stage, where the structural proof is unambiguous. However, the limited quality of the crystal did not allow for a satisfying refinement (even after disordered solvent molecules had been treated with the PLATON/SQUEEZE procedure) for publication in the CCDC. We nevertheless provide the data of the crystal as well as preliminary refinement for compound **2a**.

Crystal data

$C_{37}H_{33}BF_4Mo_2N_2O_2P_2$	$F(000) = 1760$
$M_r = 878.28$	$D_x = 1.509$ Mg m^{-3}
$a = 14.1182\ (8)$ Å	Mo $K\alpha$ radiation, $\lambda = 0.71073$ Å
$b = 15.5748\ (9)$ Å	Cell parameters from 9794 reflections
$c = 17.8932\ (11)$ Å	$\mu = 0.79$ mm^{-1}
$\alpha = 90°$	$T = 123(1)$ K
$\beta = 100.722\ (3)°$	$0.79 \times 0.55 \times 0.43$ mm
$\gamma = 90°$	space group: $P\ 2_1/n$ (No. 14)
$V = 3865.8\ (4)$ Å^3	
$Z = 4$	

Data collection

Bruker Kappa-ApexII diffractometer	$R_{int} = 0.025$
Radiation source: fine-focus sealed tube	$\theta_{max} = 25.4°$, $\theta_{min} = 1.7°$
graphite	$h = -16 \ 16$
	$k = -18 \ 18$
71871 measured reflections	$l = -21 \ 21$
7106 independent reflections	
6567 reflections with $I > 2\sigma(I)$	

Refinement

Refinement on F^2	Hydrogen site location: inferred from neighbouring sites
Least-squares matrix: full	H atoms treated by a mixture of independent and constrained refinement
$R[F^2 > 2\sigma(F^2)] = 0.069$	$w = 1/[\sigma^2(F_o^2) + (0.1197P)^2 + 55.3453P]$ where $P = (F_o^2 + 2F_c^2)/3$
$wR(F^2) = 0.223$	$(\Delta/\sigma)_{max} = 0.001$
$S = 1.08$	$\Delta\rho_{max} = 2.53$ e Å^{-3}
7106 reflections	$\Delta\rho_{min} = -4.08$ e Å^{-3}
452 parameters	Extinction correction: none
0 restraints	
0 constraints	

02. NMR Data
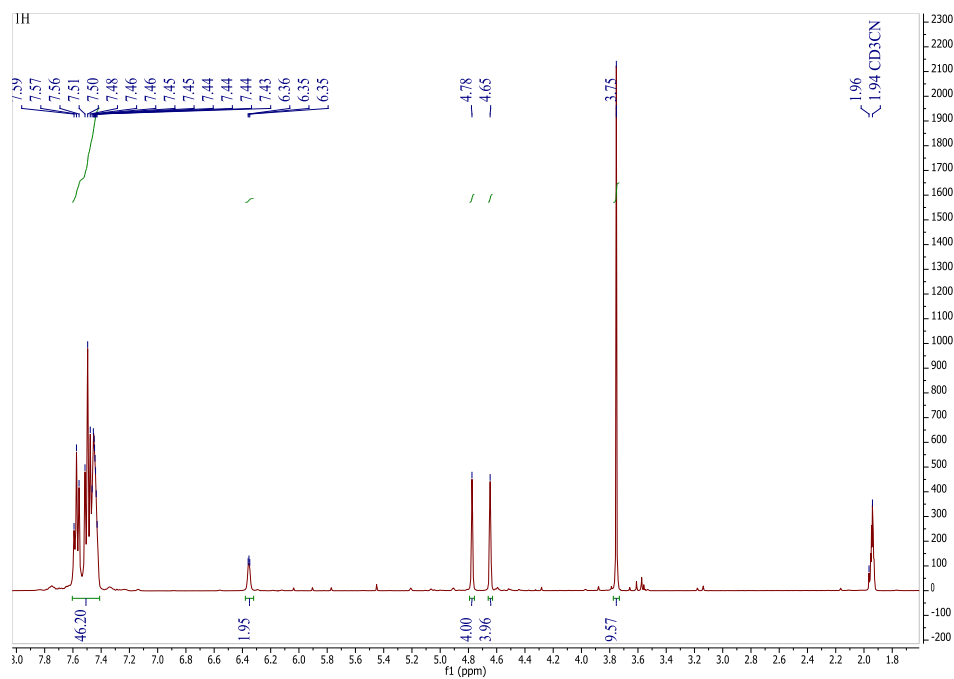
Figure S2. ^{1}H NMR spectrum of **2a** in CD$_3$CN.
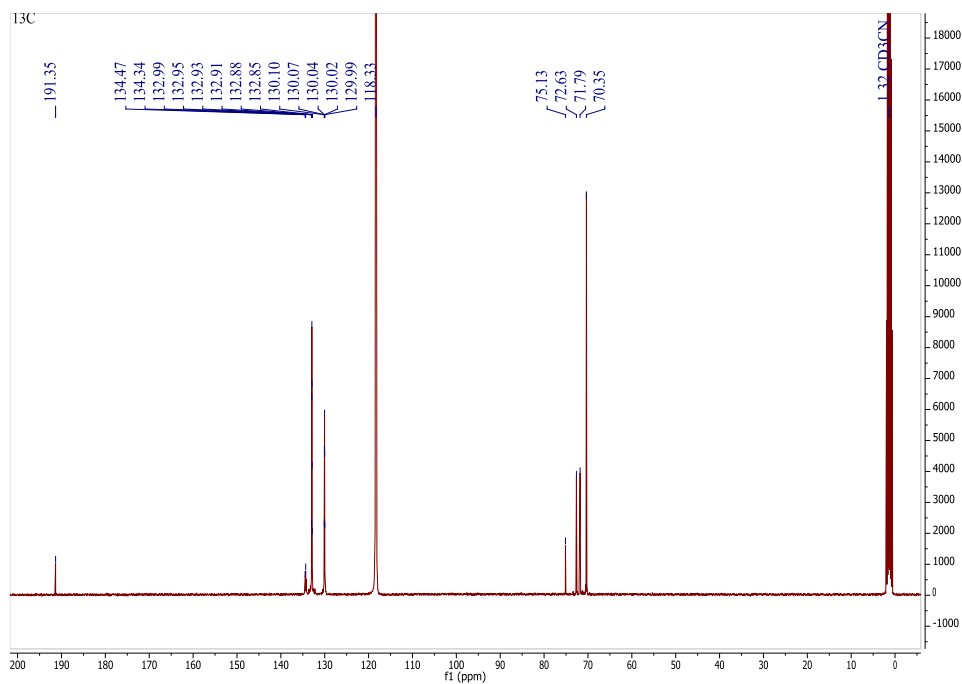
Figure S3. ^{13}C NMR spectrum of **2a** in CD$_3$CN.
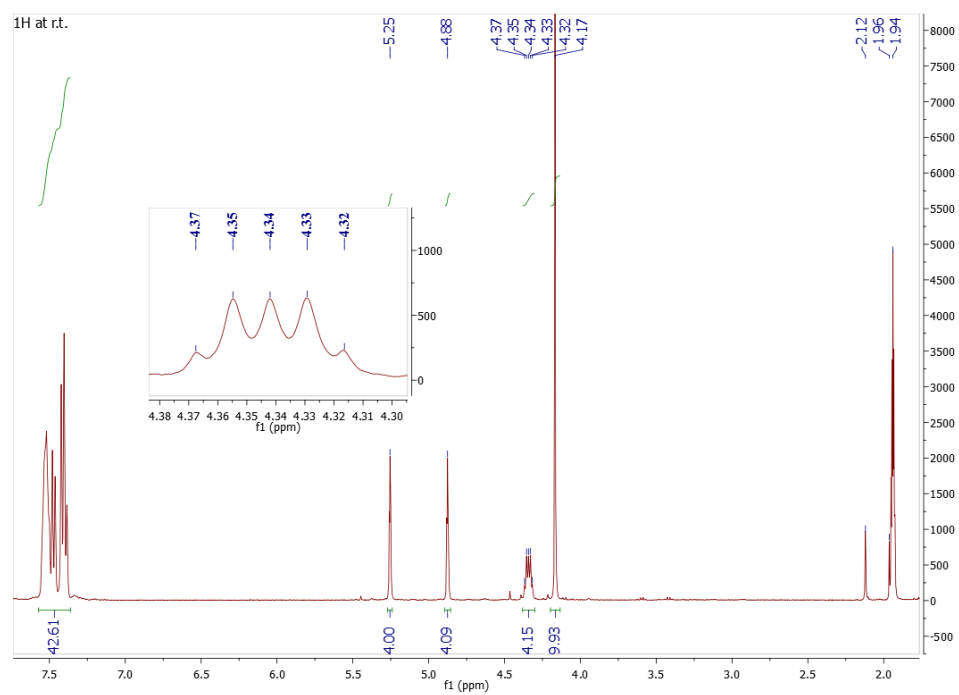
Figure S4. ^{1}H NMR spectrum of **2b** in CD$_3$CN.
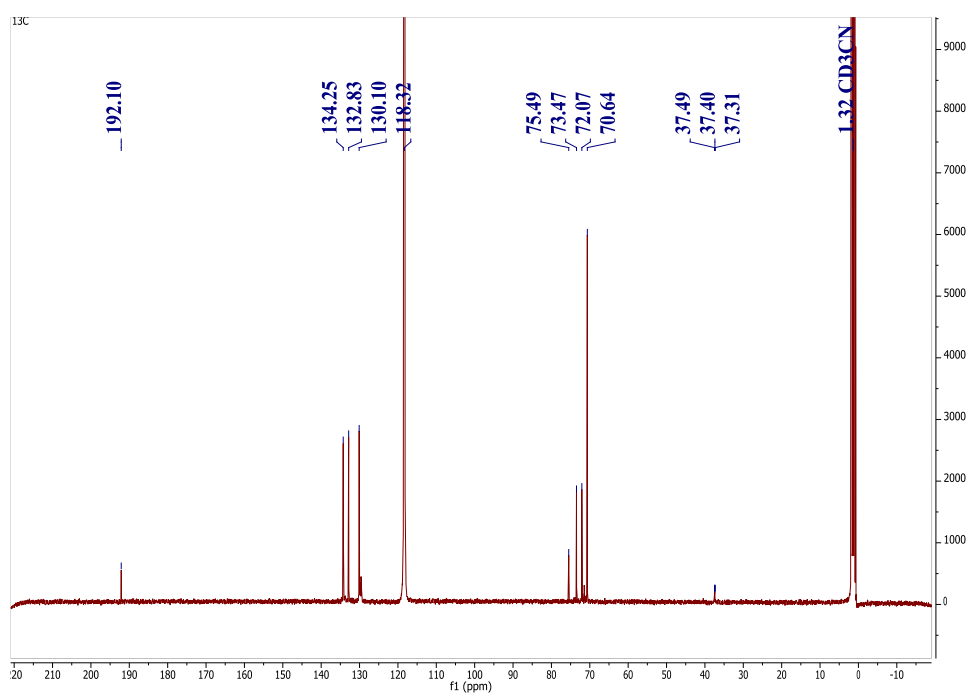
Figure S5. ^{13}C NMR spectrum of **2b** in CD$_3$CN.
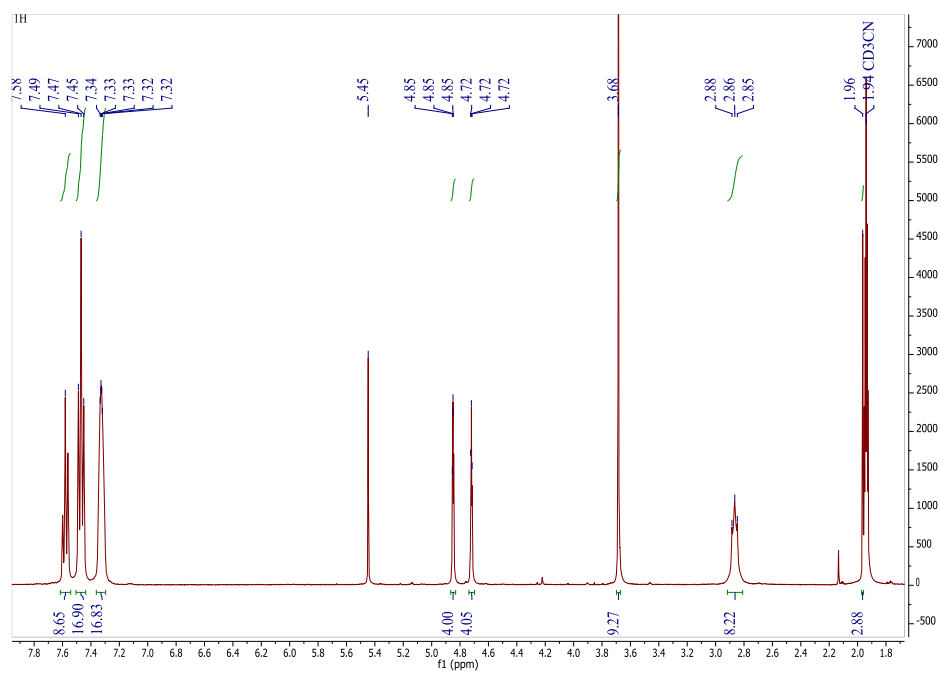
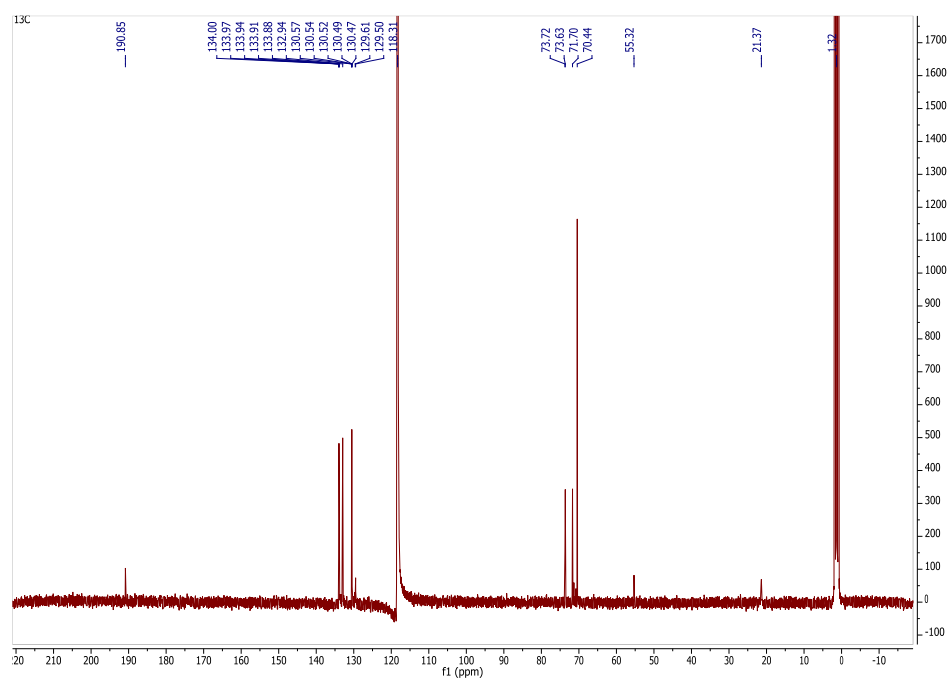**Figure S6.** ^{1}H NMR spectrum of **2c** in CD$_3$CN.

Figure S7. ^{13}C NMR spectrum of **2c** in CD$_3$CN.
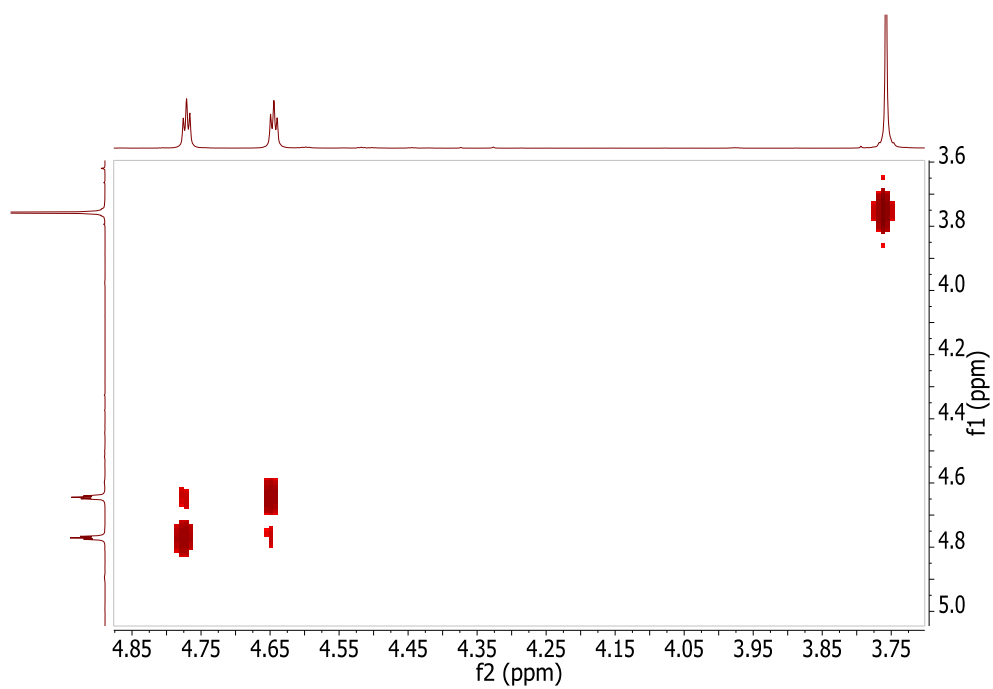
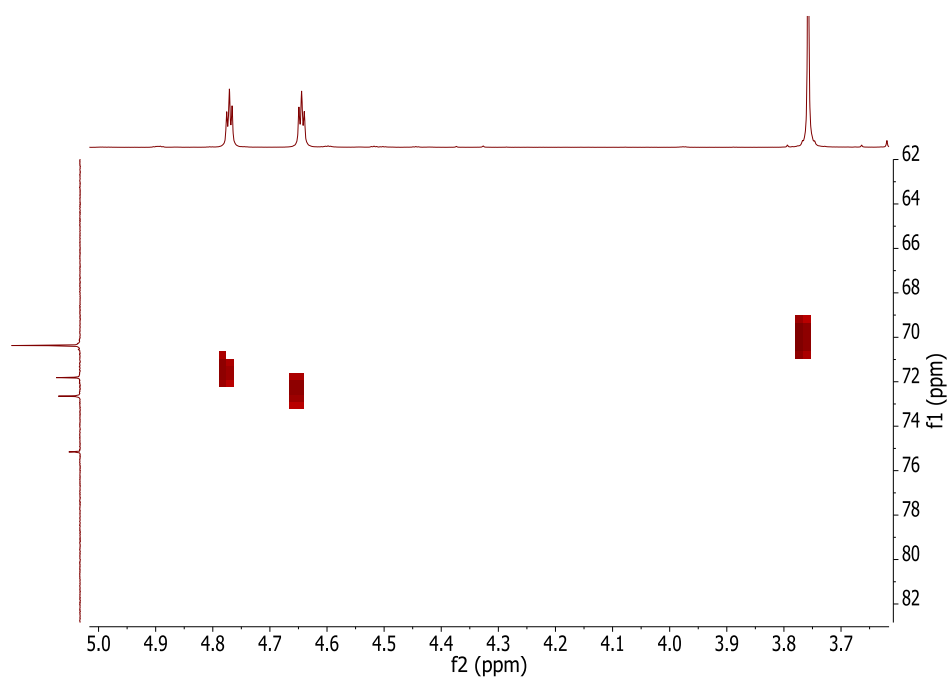**Figure S8.** Excerpt from COSY spectrum of **2a** in CD₃CN.

Figure S9. Excerpt from HSQC spectrum of **2a** in CD₃CN.
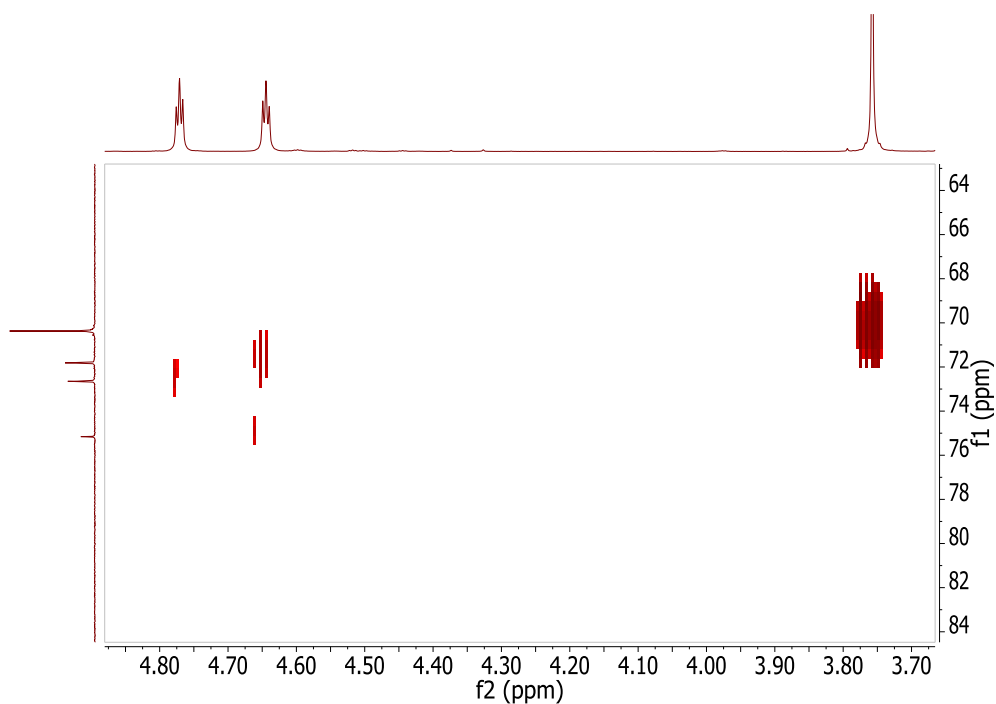
Figure S10. Excerpt from HMBC spectrum of **2a** in CD$_3$CN.

Table S1. Selected NMR signals for comparison in ppm.

Compd.	^{1}H^i (H$_a$; H$_b$; H$_c$)	Bridge-^{1}H^{ii}	^{31}P
trans-**1**	4.79; 5.20; 4.46		
DPPA		4.31	43.20
2a	4.65; 4.78; 3.75	6.33	78.45
DPPM		2.92	-23.14
2b	4.88; 5.26; 4.17	4.34	18.69
DPPE		2.06	-13.81
2c	4.72; 4.85; 3.68	2.86	20.72

[i] Proton signals on ferrocene rings. [ii] Proton signals on the bridged DPPX ligands.

Figure S11. Labelled fragment for interpretation of NMR spectra.

03. UV-Vis Data

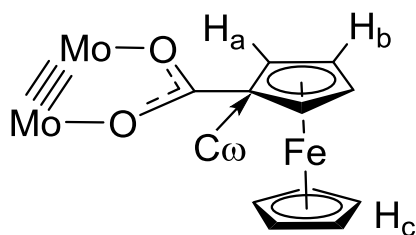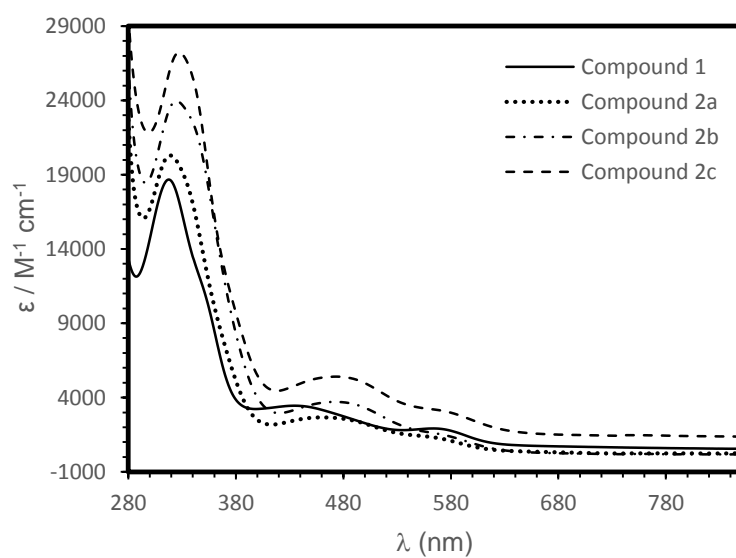**Figure S12.** Full absorption spectra of compounds **1**, **2a**-**2c** in CH_3CN.

Figure S13. Color comparison of four compounds Fc-COOH, **1**, $[Mo_2(MeCN)_{10}][BF_4]_4$ and **2a** in CH_3CN from left to right.

04. CV and DPV Data

Figure S14. Cyclic voltammograms of compounds **1** and **2a**-**2c**. Results recorded in a 0.10 M degassed CH₃CN solution of [Bu₄N][BF₄] at a scan rate of 0.2 V/s.

Figure S15. Differential pulse voltammogram of mixture *cis-* and *trans-***1**. Results recorded in a 0.10 M degassed CH₃CN solution of (*n*-Bu₄)NBF₄ at a scan rate of 0.2 V/s.

05. IR Data

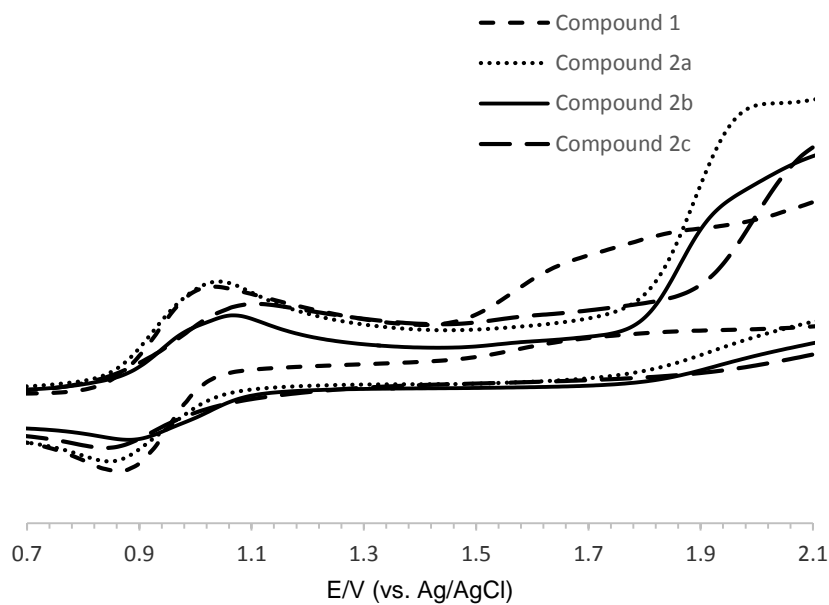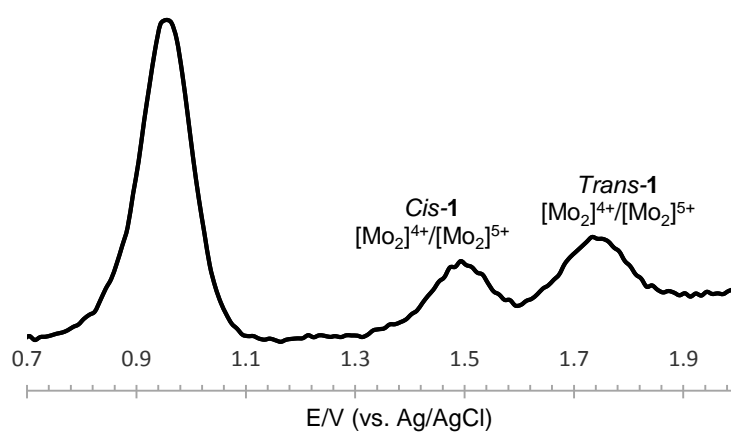Collected in Table S2 is the IR data of compounds **1** and **2a-2c** which is compared with relevant literature values. The lack of strong ν_{CN} absorption bands in products **2a-2c** - as compared to **1** - is caused by almost full decoordination of equatorial MeCN ligands due to the crowded diphosphine substitution. No detailed descriptions have been found in literature to discuss the IR spectra difference after diphosphine coordination. Nevertheless, the bridging nature can be derived from the frequency difference ($\Delta\nu$) between $\nu_{asym}(COO^-)$ and $\nu_{sym}(COO^-)$ bands of around 100 cm^{-1}.[1] The ν_{NH} absorption in compound **2a** at 3237 cm^{-1} is slightly blue-shifted compared to 3225 cm^{-1} in the free ligand DPPA. All ν_{BF} absorption bands are within the common range, just about 30 cm^{-1} blue-shifted as compared to **1**.

Table S2. Comparison of IR data.

Compound	ν_{COO} (cm^{-1})	ν_{BF} (cm^{-1})	Ref.
1	1499, 1394	1063, 1024	[2]
trans-[Mo$_2$(μ-O$_2$CCH$_3$)$_2$Cl$_2$(μ-dppma)$_2$]	1482, 1350		[3]
trans-[Mo$_2$(μ-CH$_3$CONH)(dppm)$_2$(NCCH$_3$)$_2$][BF$_4$]$_3$	1486, 1368	1084, 1062	[4]
2a	1491, 1390	1098	this paper
2b	1484, 1398	1093, 1078	this paper
2c	1487, 1390	1080, 1072	this paper

06. TG-MS Data

The masses observed via thermogravimetric analysis for compound **2a** with 11 (B), 17 (NH_3), 19 (F), 22 (B_2), 28 (CO), 31(P), 38 (F_2), 41 (CH_3CN), 44 (CO_2), 65 (C_5H_5) and 78 (C_6H_6) show full decomposition of the molecule (acetonitrile originates from residual axially coordinated ligands), indicating that the residue is mainly of metallic nature (molybdenum and iron). A similar decomposition can be observed for both compounds **2b** and **2c**. The residual mass of around 17% in compound **2a** (Figure S16) is consistent with the calculated value for the metallic moieties of 18.7%. However, both the residual masses of 35% and 24% in compounds **2b** and **2c** are higher than calculated with 18.8% and 18.2% for the metallic moieties, respectively (Figures S17 and S18). Compared to precursor **1**, TG-MS analysis of **2a** shows the mass losses at relatively high temperature ranges of 300-340 and 440-520 °C (the mass losses of **1** between 100-250 and 400-500 °C).[2] Similar mass loss trends are observed in both compounds **2b** and **2c**. More specifically, TG-MS of **2a** shows that the remaining axially-coordinated acetonitrile ligands at 310-360 and 400-600 °C, which are around 150 °C higher than for those in **1** (150-250 and 400-500 °C). The same trend can be seen in the CO_2 peak maxima of the MS curve at around 330, 489 and 665 °C, which are again higher than for those in **1** (218, 438 and 640 °C). Based on the obtained data, diphoshpine substitution results in increased temperature stability, which can be seen in all examined compounds **2b** and **2c**. Both **2b** and **2c** lose acetonitrile ligands at temperatures of 380-420/500-540 °C and 300-400/460-520 °C, respectively. The release of CO_2 in **2b** and **2c** proceeds in steps and starts at 380/512 and 360/500 °C,

respectively, proving a higher temperature stability of the carboxylate ligand compared to **1**, where CO_2 is already released in a small amount at around 218 ℃. So in general, phosphine coordination leads to higher complex stability.
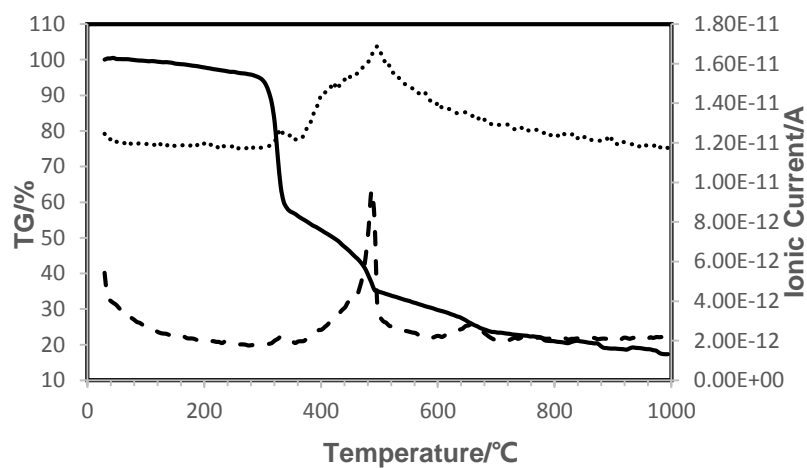

Figure S16. TG (solid) and MS curves (round dot for acetonitrile, dash for CO_2) of compound **2a**.
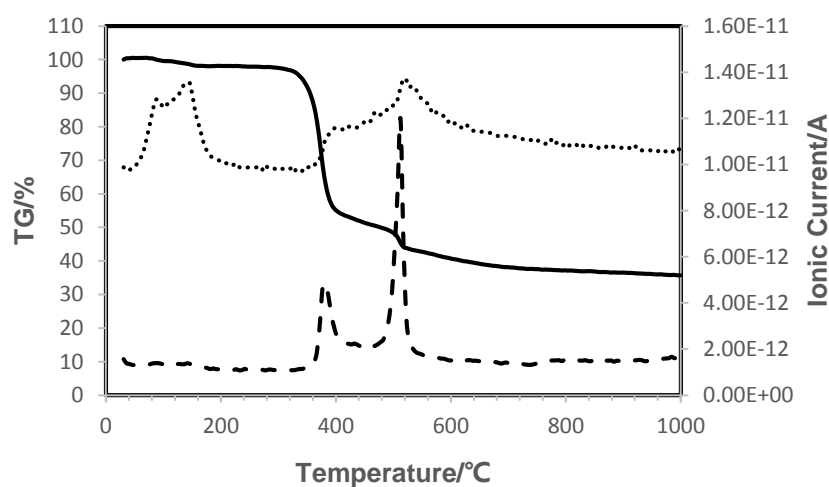

Figure S17. TG (solid) and MS curves (round dot for acetonitrile, dash for CO_2) of compound **2b**.
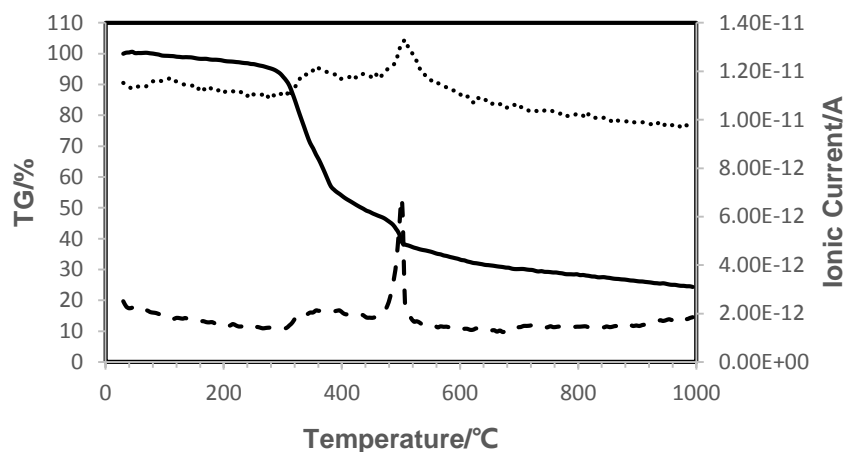
Figure S18. TG (solid) and MS curves (round dot for acetonitrile, dash for CO_2) of compound **2c**.

07. DFT Data

All Cartesian atomic coordinates for each calculated molecule can be found in the separate plain-text xyz-file.
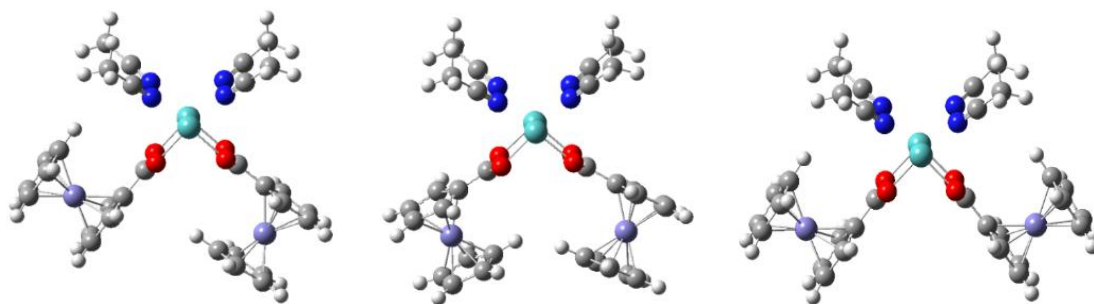
Optimized Geometries and Energies

Figure S19. Computed structures of precursor **1** (ground state, charge: +2, multiplicity: singlet): Compound **1** (left), Fc units head-to-head as **1_IN** (middle) and opposite to each other as **1_OUT** (right).

Table S3. Ground state energies of three possible species of precursor **1** in solution.

Compound	HF [Hartree]	ΔHF [kcal/mol]	G [Hartree]	ΔG [kcal/mol]
1	-4344.513586	0.000	-4344.06296	0.000
1_IN	-4344.51173	1.165	-4344.05888	2.560
1_OUT	-4344.510995	1.626	-4344.058614	2.727
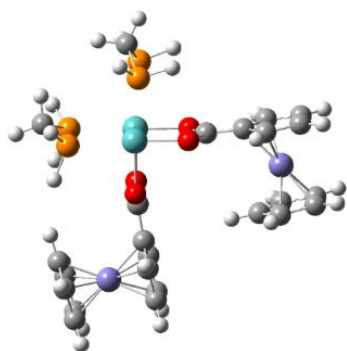
Compound **2b_H_CIS**
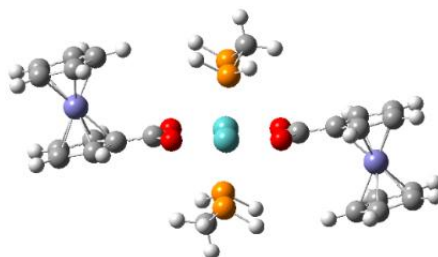
Compound **2b_H_TRANS**
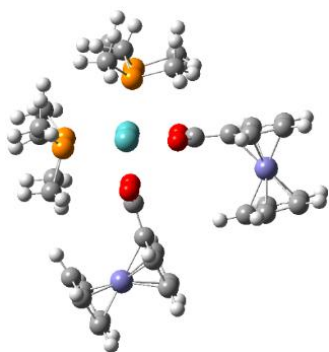
Compound **2b_Me_CIS**
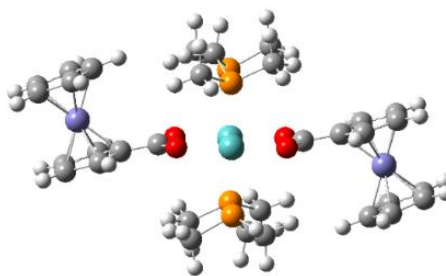
Compound **2b_Me_TRANS**

Compound **2b_Ph_CIS**

Compound **2b**

Figure S20. *Cis-* and *trans-*paired structures with R groups from H to methyl to phenyl (ground state, charge: +2, multiplicity: singlet; **2b** refers to compound in the manuscript, would otherwise be named compound **2_Ph_TRANS**).

Table S4. Ground state energies for all diphosphine-coordinated complexes with R groups from H to methyl to phenyl.
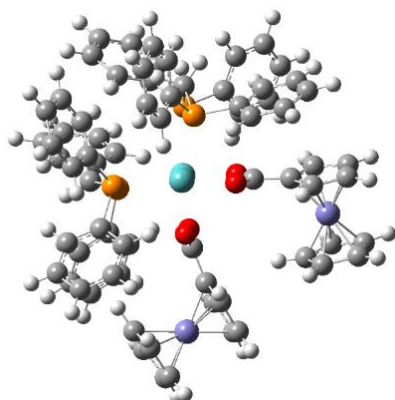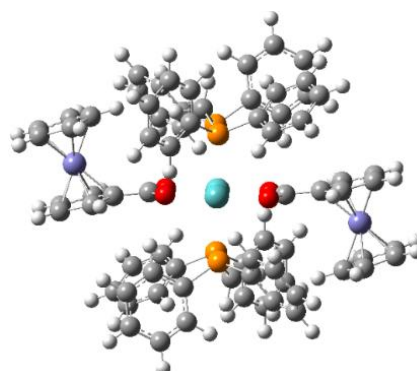
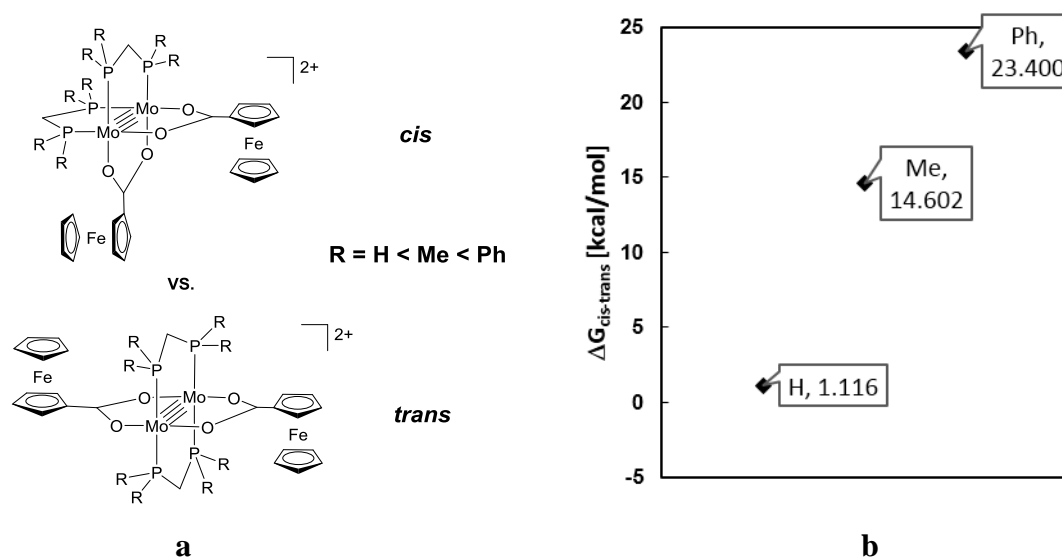| Compound	HF [Hartree]	$\Delta HF_{cis\text{-}trans}$ [kcal/mol]	G [Hartree]	$\Delta G_{cis\text{-}trans}$ [kcal/mol]
2b_H_CIS	-5262.2624866	-0.253	-5261.8482	1.116
2b_H_TRANS	-5262.2620830		-5261.8500	
2b_Me_CIS	-5576.7520599	10.166	-5576.116162	14.602
2b_Me_TRANS	-5576.7682604		-5576.139431	
2b_Ph_CIS	-7110.0434058	20.519	-7109.016652	23.400
2b	-7110.0761043		-7109.053943	

Figure S21. a) *Cis-* and *trans*-structures via diphosphine coordination. b) $\Delta G_{cis\text{-}trans}$ diagram for diphosphine-coordinated complexes with R groups from H to methyl to phenyl.

MO Energies

Table S5. Molecular orbital energies for compounds **1** and **2a-c**.

| in eV	Compound **1**	Compound **2a**	Compound **2b**	Compound **2c**
LUMO+5	-5,96	-5,47	-5,50	-5,36
LUMO+4	-6,04	-5,66	-5,66	-5,50
LUMO+3	-6,12	-6,01	-5,85	-5,63
LUMO+2	-6,86	-6,10	-5,88	-5,90
LUMO+1	-6,97	-6,15	-6,01	-6,10
LUMO	-8,08	-7,21	-7,18	-7,05
HOMO	-8,93	-8,65	-8,73	-8,65
HOMO-1	-8,98	-8,65	-8,76	-8,65
HOMO-2	-9,14	-8,65	-8,76	-8,65
HOMO-3	-9,17	-8,71	-8,79	-8,71
HOMO-4	-9,33	-9,06	-9,14	-9,06
HOMO-5	-9,55	-9,06	-9,17	-9,09

TD-DFT Data

HOMO corresponds to MO#174 in compound **1**, to MO#332 in compounds **2a/b** and to MO#340 in compound **2c**.

Table S6. Predicted excited states with respective oscillation strengths, transitions and contributions for compounds **1** and **2a-c**.

	λ [nm]	O. S.	E [eV]	from MO#	to MO#	Contribution
Compound 1	409.5	0.0126	3.028	171	181	66%
				173	184	12%
	492.4	0.0269	2.518	171	180	50%
				171	184	17%
				171	195	20%
				172	192	15%
	502.1	0.0351	2.469	170	181	17%
				173	181	51%
				173	184	21%
				173	186	17%
Compound 2a	484.4	0.0431	2.560	329	342	21%
				329	344	23%
				329	363	16%
				330	340	28%
				332	340	37%
				332	361	11%
	584.6	0.0118		326	333	69%
Compound 2b	485.8	0.0461	2.552	327	342	12%
				329	344	15%
				330	338	19%
				330	356	10%
				331	357	13%
				332	338	39%
				332	359	16%
	577.4	0.0124		326	333	69%
Compound 2c	483.4	0.0390	2.565	335	350	12%
				336	346	11%
				337	350	26%
				337	368	14%
				339	365	11%
				340	346	39%
				340	367	13%
	588.2	0.0171	2.108	334	341	67%
				340	342	13%

Additional MO Plots

Compound **2b**: HOMO (ground state, charge: +2, multiplicity: singlet)
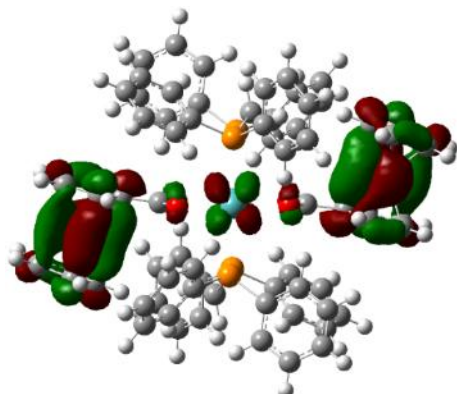
Compound **2c**: HOMO (ground state, charge: +2, multiplicity: singlet)
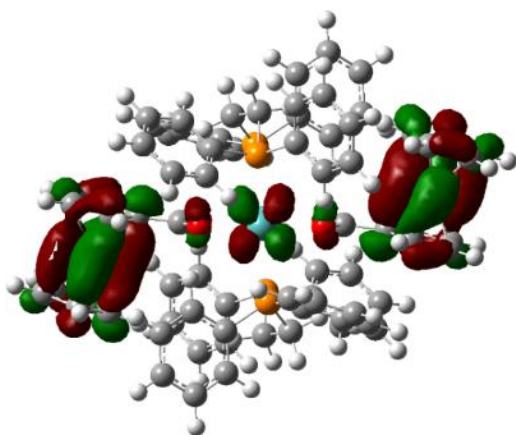
08. References

(1)   Socrates, G. *Infrared and Raman Characteristic Group Frequencies: Tables and Charts*; Wiley, 2004, 133-134.

(2)   Cai, X.-M.; Höhne, D.; Köberl, M.; Cokoja, M.; Pöthig, A.; Herdtweck, E.; Haslinger, S.; Herrmann, W. A.; Kühn, F. E. *Organometallics* **2013**, *32*, 6004-6011.

(3)   Cotton, F. A.; Kühn, F. E.; Yokochi, A. *Inorg. Chim. Acta* **1996**, *252*, 251-256.

(4)   Cotton, F. A.; Daniels, L. M.; Haefner, S. C.; Kühn, F. E. *Inorg. Chim. Acta* **1999**, *287*, 159-166.